神戸大学都市安全研究センター
研究報告，第20号，平成28年３月

# SUBDUCTION DYNAMICS AND MANTLE TOMOGRAPHY BENEATH JAPAN

Vlad Constantin MANEA 1)
Shoichi YOSHIOKA 2)
Marina MANEA 3)

Abstract: Tomographic images of the Japanese subduction zone revealed that most of the Pacific subducting oceanic plate does not penetrate into the lower mantle; rather it stagnates in the transition zone for a long distance of 800 km or more. Observations of subduction characteristics, as convergence rates, plate ages and trench migration rates do not exhibit a clear correlation with the slab morphology, especially in the transition zone. In this study we employed large scale 3D dynamic numeric modeling in order to investigate the influence of trench migration rates on the interaction between the Pacific slab with the transition zone and lower mantle. Numeric modeling of subduction that have been integrated for 20 Myr show that slab stagnation, or flattening, along the transition zone are greatly facilitated through progressive trench retreat. On the other hand, the subducting slab can penetrate into the lower mantle for modeling scenarios that incorporate gradual trench retreat. When comparing the modeling trench rates with observation of present-day trench migration rates, we observed some large differences between the modeling results and slab geometries from mantle tomography. This suggests that transition zone stagnating slabs probably have different subduction zone characteristics than other slabs, which are not easily explained by simple dynamical models that do not include the specific tectonic history of the entire subduction system. This is the initial effort to understand the long-term geodynamics of the Japanese subduction system, and future studies will focus on incorporating into numeric models realistic paleoreconstructions models.

Key words: Numeric modeling, Seismic tomography, Subduction zones, Subducting oceanic plates and Mantle transition zone.

## 1. INTRODUCTION

It is generally accepted that convection inside the Earth and therefore flow in the mantle is strongly influenced by the subduction of dense oceanic lithosphere (Forsyth & Uyeda 1975; Zhong & Gurnis 1995). Mantle tomographic images revealed that the greatest seismic anomalies are actually associated with subducting slabs, which are clearly detectable down to at least the 660-km seismic discontinuity. An interesting aspect related with subducting slabs is their great variability, both in geometry as well as distribution of seismicity. Despite a smooth and gradual variation of subduction parameters, slab geometry is observed to vary greatly along the strike in a variety of local subduction settings, including the Japan subduction zone (Figure 1). The three-dimensionality in slab structure can play an important role on the relative motion of the surrounding mantle, as can be seen in recent studies of seismic anisotropy (Kaneshima and Ando, 1989; Kaneshima, 1990; Nakajima and Hasegawa, 2004; Nakajima *et al.*, 2006). Additionally, three-dimensionality of slab structure can have a strong impact on the distribution and intensity of intraslab earthquakes.

The Japanese subduction zone is one of the few regions in the world where long term subduction of old lithosphere (>120 Ma) happens at high rates ~9 cm/yr (Lallemand *et al.*, 2005). Here the Pacific slab sinks into the upper mantle beneath central Japan at a shallow angle of ~20° for a distance of ~800 km before is reaching the mantle transition zone (Figure 1). At a depth of ~660 km, the slab stagnates and lies horizontally for several hundreds of kilometers (Niu *et al.*, 2005) The geodynamical origin of the Japanese subduction zone based on such contrasting information is not yet fully understood (Billen, 2010), and this study represents one of the first steps in finding the first order cause of the Pacific stagnant slab in particular, but in the same time, plays an important role in understanding long-term geodynamical evolution of subduction zones in general. For this purpose we use 3D dynamic numeric modeling technique to investigate the impact of subducting slabs with the 410-km and 660-km seismic discontinuities. Finally, we assess the modeling results with tomographic images of the subducting slab beneath Japan and discuss the implication of different sets of boundary conditions applied on tops of the models as plate velocities.

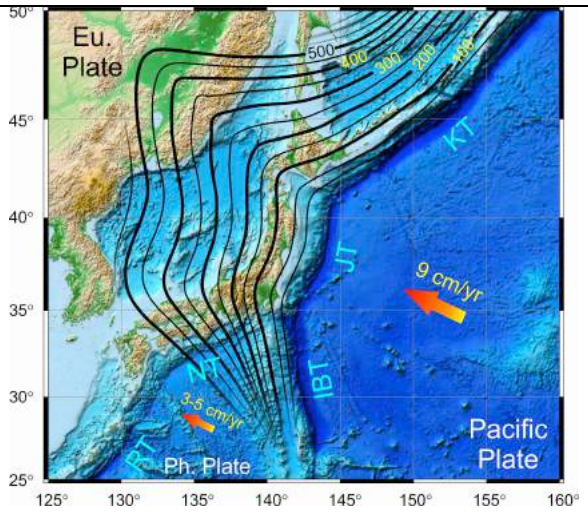


Figure 1. Topographic and bathymetric map of the Japanese subduction zone. Black curves represent Benioff zone isodepths (Gudmundsson & Sambridge 1998). Red arrows show the direction Pacific and Philippine plates motion as given by the HS3-Nuvel1A model (Gripp and Gordon, 2002). IBT-Izu Bonin trench, JT-Japan trench, KT-Kurile trench, NT-Nankai trough, and RT-Ryukyu trench. Eu. Plate –Eurasian plate, Ph. Plate-Philippine Sea plate.

## 2. METHODOLOGY

### 2.1 Study area

Japan is located above an active subduction zone where both Pacific and Philippine Sea plates are currently subducting beneath the Eurasian plate at a rate of 8–9 cm/yr and 3-5 cm/yr respectively (Figure 1). The Pacific plate is being subducted beneath northeast Japan along the Kuril and Japan trenches, and beneath the Philippine Sea plate along the Izu-Bonin trench (Figure 1). On the other hand, the Philippine Sea plate is being subducted beneath southeast Japan along the Suruga-Nankai trough and the Ryukyu trench, respectively (Figure 1). Because of this complex and fast subduction system, earthquakes are caused by the active subduction and collisions among three major tectonic plates as the Pacific, Philippine Sea, and Eurasian plates (Figure 1) (Hasegawa *et al.*, 2009). Large interplate and intraplate earthquakes occur actively in the forearc region, upper crust, as well as within the subducting Pacific plate at greater depths, from which Japan suffered heavily from seismic hazards during the long history (Utsu, 1982; Usami, 2003). Since there is strong spatial correlation between the large subduction earthquakes ($M_w$>6.0) and the structural heterogeneities in the crust and the mantle, the accuracy of earthquake distribution in a subduction zone represents a key for obtaining a robust seismic tomography (Zhao *et al.*, 2002, 2010). Figure 2 shows the seismicity distribution associated with the Japan subducting system and plate boundaries, where seismic activity reaches as deep as ~600 km within the subducted Pacific plate, and as deep as ~300 km in the subducted Philippine Sea plate.

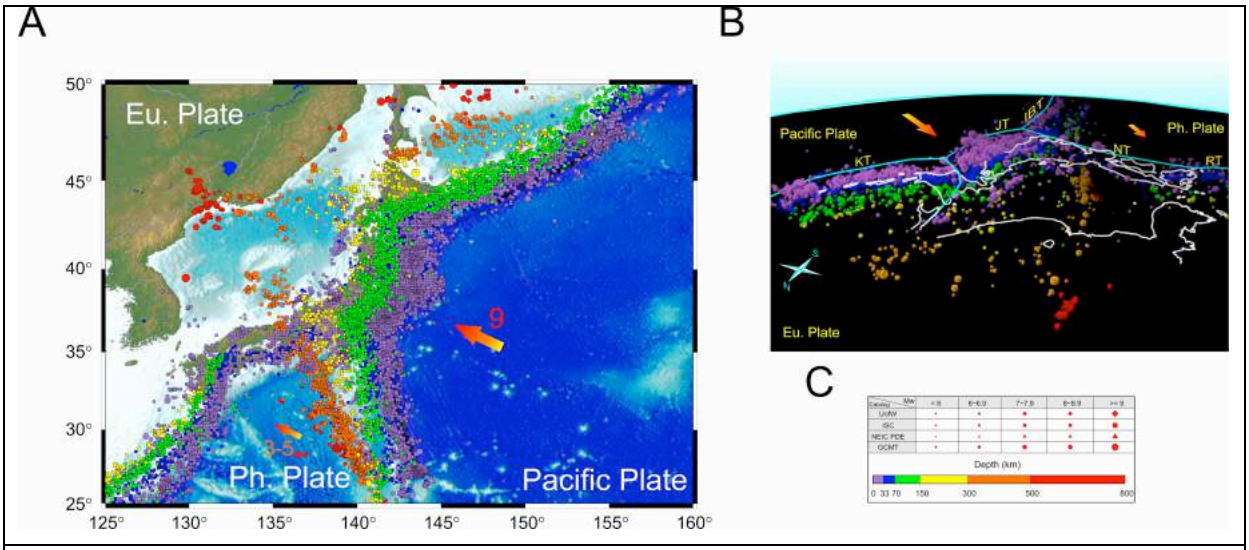


Figure 2. A. Seismic events map ($M_w$>3) associated with the Japan subduction zone based on data from several sources including USGS, GCMT, NEIC and ISC dating from 1960 to the present. B. 3D view of the seismic event distribution. C. Event size and colors are depth based according with the table.

### 2.2 Mantle tomography

Seismic tomography revealed that the sinking subducting slabs often stagnate in the lower part of the mantle transition zone where is known that rocks undergo pressure-induced phase transitions. In Japan the detection and analysis of converted and reflected waves (Hasegawa *et al.*, 1978; Matsuzawa *et al.*, 1986, 1990; Fukao *et al.*, 1992, 2001, 2010; Zhao *et al.*, 1997) clearly revealed the Pacific subducting slab by a high P-wave velocity contrast between the slab and the mantle wedge. Since in this study we focus on the evolution of the subducting Pacific plate beneath Japan, we select three tomographic cross-sections that cover the three different Pacific trench segments, the Izu-Bonin, Japan, and Kurile trenches (Figure 3). The large-scale mantle tomography images presented in Figure 3 reveal some of the first-order features of the Japan subduction zone as the high-velocity subducting Pacific slab. The seismic tomographic image beneath the Kurile to Bonin arcs, shows that the subducting Pacific slab bends to subhorizontal in the mantle transition zone and extends continentward over a great distance of ~1000 km or more (Fukao *et al.*, 1992). This is a common feature observed in all three cross-sections, but is more noticeable for the Pacific plate subducting along the Izu Bonin and Japan trenches (Figure 3). On the other hand, the Pacific slab beneath northern Japan, which is the subducting plate dips into the upper mantle at a steep angle, but is able to penetrate into the lower mantle but for only 100-200 km. Additionally, the high-velocity anomaly located on top of the lower mantle probably suggests that the Pacific slab has stayed in the past into the transition zone (Figure 3 – cross-section A-A').

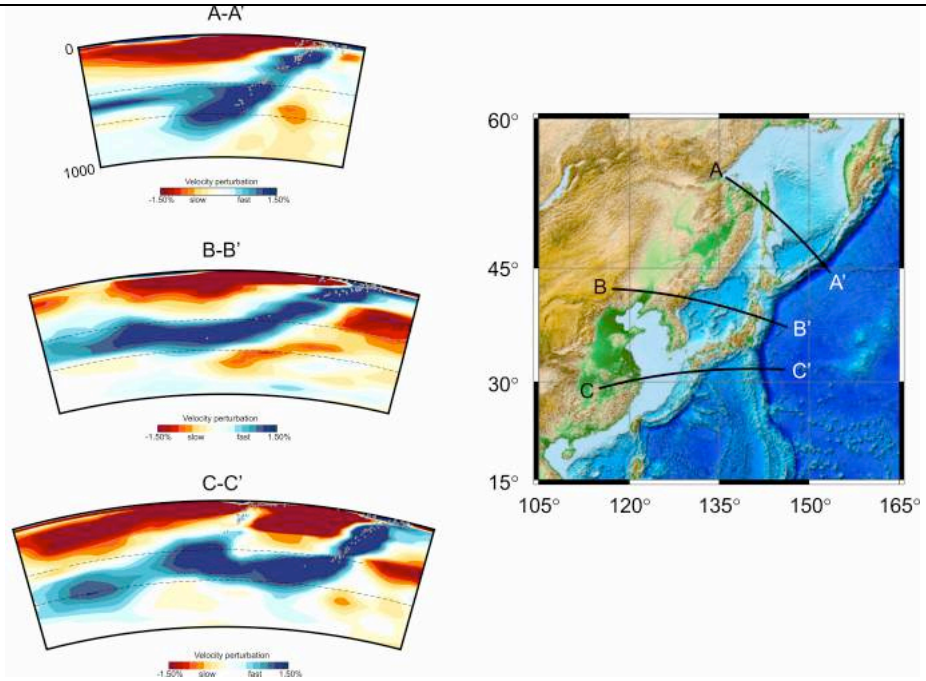


Figure 3. P-wave velocity contrast beneath Japan where the Pacific (cross sections A-A' and B-B') and Philippine Sea (cross section C-C') slabs are revealed by a high P-wave velocity contrast. Blue colors represent faster than average seismic velocities, which are related to the colder subducting Pacific and Philippine Sea slabs. Gray dots shown in cross-sections represent the Pacific and Philippine Sea slab seismicity. Dashed black curves in cross-sections represent the 410-km and 660-km seismic discontinuities. Continuous black curves shown on the map represent the location of the three cross-sections.

### 2.3 Numerical method and model setup

Mantle convection is governed by the coupling between fluid flow and energy transport and the numeric calculations are performed in a 3-D cut through a sphere on a non-deforming grid, by solving the conservation equations of mass, momentum and energy under the Truncated Anelastic Liquid Approximation which includes dissipative heating in the energy equation (Tan *et al.,* 2006). Using the incompressible version of the finite element package *CitcomS* (Zhong *et al.*, 2000; Tan *et al.*, 2006), the computations are performed within a large spherical domain ($r, \phi, \theta$), where r is radius, $\phi$ is longitude and $\theta$ is latitude. The inner radius corresponds to a depth of 1900 km, and the outer radius corresponds to the surface of the Earth. The span in longitude is 1 radian, and 0.5 radians in latitude (Figure 3A). We kept constant all boundary and initial conditions along the strike ($\theta$ direction). This domain is unevenly divided into 128 elements in the radial direction, and evenly divided into 512 elements in longitude, and 256 elements in latitude, corresponding to (10-15) x 12 x 12 km resolution. The boundary conditions are as follows: the top and bottom boundaries are isothermal, and the lateral boundaries are reflective; the top boundary has an imposed velocity boundary condition as following: $V_{OC}$ is the velocity of the oceanic plate, $V_C$ is the velocity of the continental plate, and $V_t$ is the velocity of the trench which in our models is the same as the $V_C$ (Figure 3A). The bottom is free slip, and the sides are reflecting. The initial thermal

structure is described by an age controlled thermal boundary layer (100 Ma for the oceanic plate and 20 Ma for the continental plate) at the top and isothermal mantle with an initial slab with ~45°dip angle (Figure 3B). We placed ~1.5 million tracers on top of the oceanic plate (Figure 3C) to track the slab surface and also to impose on top of the slab surface a low viscosity channel (40 km thick) and low viscosity wedge down to a depth of 300 km (Figure 3D) (Manea and Gurnis, 2007).

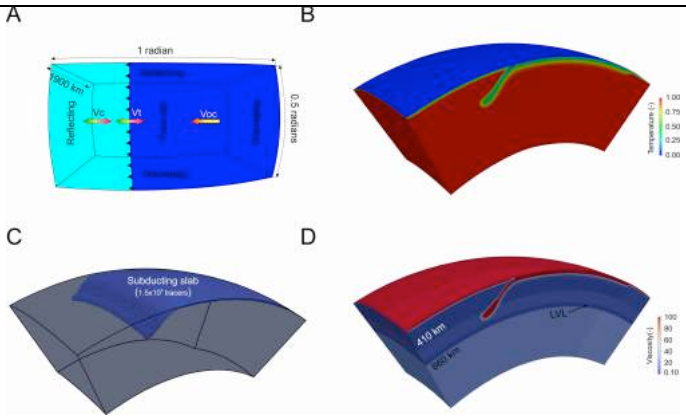


Figure 3. Initial model configuration and boundary conditions. A: Model dimensions and boundary conditions. B: Initial temperature distribution. The slab dips at ~45° and penetrates the 410 km discontinuity. C: The initial oceanic slab surface is defined by ~1.5 million tracers (colored in blue). D: Initial viscosity distribution. The model incorporates a low viscosity wedge and channel (viscosity drop of one order of magnitude in respect with the upper mantle). Also we include a 100 km thick low viscosity layer (LVL) on top of the 660 km depth discontinuity.

In these models we varied systematically $V_{OC}$, $V_C$ and $V_t$, and all the other parameters that are held constant are summarized in Table 1. The equations are written in non-dimension form as following:

$$(u_i)_{,i} = 0 \tag{1}$$

$$-P_{,i} + \eta(u_{i,j} + u_{j,i})_{,j} + \delta\rho g \delta_{ir} = 0 \tag{2}$$

$$T_{,t} + u_i T_{,i} = kT_{,ii} + H \tag{3}$$

where, $u_i$ is the velocity, $P$ is the dynamic pressure, $Ra$ is the Rayleigh number, $\eta$ is the viscosity, $\delta_{ij}$ is the Kronecker delta tensor, $\delta_\rho$ is the density anomaly, $T$ is the temperature, $T_0$ is the temperature at surface, $\delta\rho$ is the density anomaly, $cp$ is the heat capacity, $k$ is the thermal diffusivity, $\alpha$ is the thermal expansivity, $\Phi$ is the viscous dissipation, $Q_L$ is the latent heat, and $H$ is the heat production rate. The expression $X_{,y}$ represents the derivative of $X$ with respect to $y$, where $i$ and $j$ are spatial indices, $r$ is the radial direction, and $t$ is time.

Table 1. A list of parameters that are held constant in our numeric models. Reference values can be used to convert non-dimensional parameters into dimensional ones.

| **Parameter** | **Symbol** | **Value** | **Dimension** |
|---|---|---|---|
| Reference temperature | $T_0$ | 1350 | °C |
| Reference viscosity | $\eta_0$ | $1x10^{21}$ | Pa s |
| Thermal expansion coefficient | $\alpha$ | $2x10^{-5}$ | 1/K |
| Gravitational acceleration | $g$ | 10 | $m/s^2$ |
| Thermal diffusivity | $k$ | $1x10^{-6}$ | $m^{2/}s$ |
| Heat capacity | $c_p$ | 1200 | J/kg K |
| Internal heating number | $H$ | $1.6\ x10^{12}$ | W/kg |
| Clapeyron slope 410 phase transition | $\gamma_{410}$ | 3.5 | MPa/K |
| Clapeyron slope 660 phase transition | $\gamma_{660}$ | -3.5 | MPa/K |
| Width of the 410 km phase transition | $\delta w_{410}$ | $37x10^3$ | m |
| Width of the 660 km phase transition | $\delta w_{660}$ | $37x10^3$ | m |
| Ambient temperature of the 410 km phase change | $T_{410}$ | 0.78x $T_0$ | °C |
| Ambient temperature of the 660 km phase change | $T_{660}$ | 0.87x $T_0$ | °C |

Our models also incorporate phase changes at 410 km and 660 km discontinuities and densities anomalies due to temperature and phase transitions are calculated as:

$$\delta\rho = -\alpha\,\bar{\rho}(T - \bar{T}_a) + \delta\rho_{ph}\Gamma \tag{4}$$

where $\bar{\rho}$ is the radial profile of density, $\alpha$ is the coefficient of thermal expansion, $\bar{T}_a$ is the radial profile of adiabatic temperature, $\delta\rho_{ph}$ is the density jump across the phase change, and $\Gamma$ is the phase function, defined as following:

$$\Gamma = \frac{1}{2}\left(1 + \tanh\left(\frac{\pi}{\bar{\rho} g w_{ph}}\right)\right) \tag{5}$$

$$\pi = \bar{\rho}\, g(1 - r - d_{ph}) - \gamma_{ph}\left(T - T_{ph}\right) \tag{6}$$

where π is the reduced pressure, $d_{ph}$ and $T_{ph}$ are the ambient depth and temperature of phase change at 410 km or 670 km depth, $\gamma_{ph}$ is the Clapeyron slope of the phase change, and $w_{ph}$ is the width of the phase transition. In our models we used a Clapeyron slope of +3.5 MPa/K (density jump: +9%) at 410 km, and of -3.5 MPa/K (density jump: -9%) at 660 km depth.

The oceanic plate has a constant thickness of 100 km, has a thermal age of 90 Myr and has a velocity of 9 cm/yr. The continental plate has a smaller thickness of 50 km and a thermal age of 20 Myr. The velocity imposed to the continental plate (and the trench) is tested in our models from -2 cm/yr (trench retreat) to +2 cm/yr (trench advance). The viscosity contrast between the oceanic and continental plates and the upper mantle is $10^2$. The maximum viscosity contrast between the upper mantle and the mantle wedge is also $10^2$, giving a viscosity variation of $10^3$ across the whole computational domain. We used the upper mantle as a reference viscosity layer (non-dimensional viscosity of 1). The transition zone has a viscosity 5 time higher than the upper mantle, and the lower mantle has a viscosity 20 times higher that the upper mantle (Figure 3D). Following Yoshioka and Naganoda (2010) we also incorporate in our models a 100 km thick low viscosity layer (LVL) (0.1 times of the upper mantle) located on top of the 660 km depth discontinuity (Figure 3D).

## 3. MODELING RESULTS

By integrating Pacific plate kinematics forward for 20 Myr, we investigated the interaction between the subducting slab with the upper and lower mantle, as well as with the transition zone. While the top velocity boundary conditions for the oceanic plate are held fixed at 9 cm/yr, we investigate the influence of trench velocity on the time-space evolution of subduction zone. All the models start from the same initial model that is a initial slab which reaches a depth of ~500 km (Figure 3). We varied the trench velocity from -2 cm/yr (trench advance) to +2 cm/yr (trench retreat) in steps of 1 cm/yr, and find that trench velocity has a dramatic effect on subduction zone structure, including slab geometry. For the first 5 Myr of evolution, the overall slab behavior is approximately independent of trench velocity and direction of movement (advance or retreat) (Figure 4). However, after 10 Myr of subduction the slab structure changed significantly. As the trench velocity increases, the slab dips into the upper mantle more gradually until it reaches the transition zone. Here the slab is not able to penetrate the lower mantle, and stagnates and progressively moves along the transition zone (Figure 5). At smaller rates of trench retreat (<1 cm/yr), the slab seems to accumulate in the transition zone and eventually will penetrate into the lower mantle (Figure 5). However when the trench retreats at higher rates (>1 cm/yr) the smaller resistance of the low viscosity layer facilitates the movement of the slab along the transition zone for hundreds of kilometers.

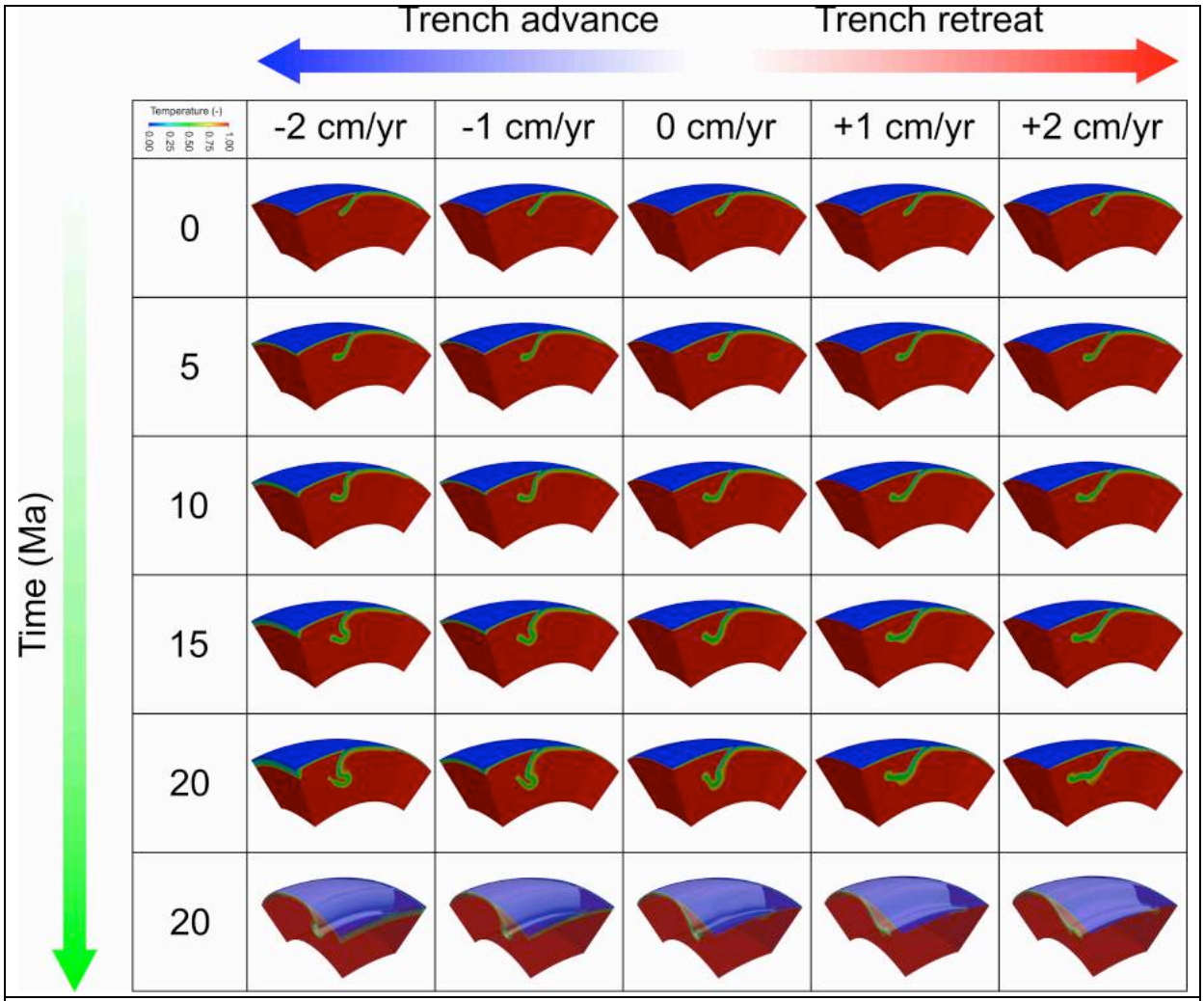


Figure 4. Time evolution of the temperature field for model runs depending on the trench velocity (retreat or advance). The last row shows a 3D view of the model after 20 Myr of evolution. The semitransparent surfaces represent the isosurface for a non-dimensional temperature of 0.5.

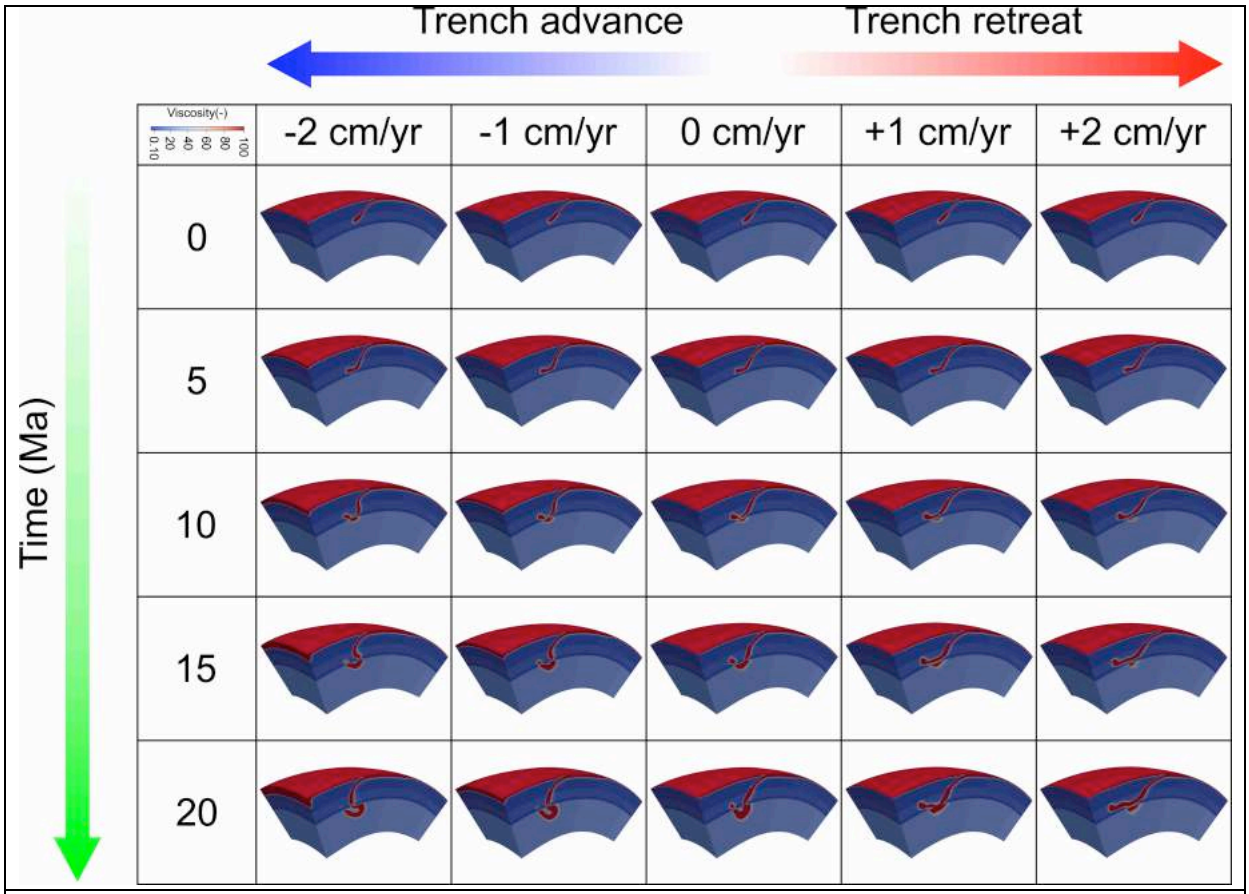


Figure 5. Time evolution of the viscosity field for model runs depending on the trench velocity (retreat or advance).

## 4. CONCLUSIONS

In this study we employed a systematic sequence of trench migration rates, from trench advance to trench retreat, to investigate some of the major controls upon transition zone slab deformation and its interaction with the lower mantle. This methodology permitted us to qualitatively and quantitatively brings to bear as main constraint tomographic images of the subducting Pacific slab. From this comparison of observations with model predictions, it appears that the dynamics of slabs is profoundly influenced by the trench migration rates (Figure 4,5).

The best models that fit tomographic images across A-A', B-B' and C-C', are all trench retreat models with 1-2 cm/yr rates. However, when comparing the modeling trench rates with present-day trench migration rates we observed some large discrepancies. Only for cross-section A-A', the present-day trench retreat rate of ~+1.5 cm/yr is in good agreement with the numeric model corresponding to a trench retreat rate of +1 cm/yr. For the other two cross-sections (B-B' and C'C') which are currently in a trench advance mode, our model results (Figure 4,5) do not fit the actual slab geometries. On the contrary, our best fitting models are those with a rather high rate of trench retreat of +2cm/yr.

This is the initial effort to understand the long-term geodynamics of the Japanese subduction system, and this study will be of valuable importance of further advancing in understanding the evolution of this complex subduction region.

**ACKNOWLEDGEMENT**

Support from the Research Center for Urban Safety and Security, Kobe University, Japan enabled the successful development of the numerical models and the access to valuable geophysical data. Numerical computations were performed at the Computational Geodynamics Laboratory – Geosciences Center, National Autonomous University of Mexico (UNAM) supercomputing facility Horus. The authors also would like to acknowledge the supports obtained from the DGAPA-PASPA-UNAM Mexico for providing the research funding and the travel expenses, respectively, to the third author to conduct numerical simulations pertinent to the project.

**REFERENCES**

Billen, M. Slab dynamics in the transition zone. Physics of the Earth and Planetary Interiors 183(1-2): 296-308. 2010.

Forsyth, D.W. and Uyeda, S. On the relative importance of the driving forces of plate motion. Geophysical Journal of the Royal Astronomical Society 43(1): 163-200, 1975.

Fukao, Y., Obayashi, M., Inoue, H., and Nenbai, M. Subducting slabs stagnant in the mantle transition zone, J. Geophys. Res. 97(B4): 4809–4822, 1992.

Fukao, Y., Widiyantoro, S., and Obayashi, M. Stagnant slabs in the upper and lower mantle transition region, Rev. Geophys., 39, 291–323, 2001.

Fukao Y.K., Nishida K., Kobayashi N. Seafloor topography, ocean infragravity waves, and background Love and Rayleigh waves. Journal of Geophysical Research, 115:B04302, 2010.

Gripp, A.E., and Gordon, R.G. Young tracks of hotspots and current plate velocities. Geophys. J. Int., 150(2), 321-361, 2002.

Gudmundsson, Ó., and Sambridge, M. A regionalized upper mantle (RUM) seismic model, J. Geophys. Res., 103(B4), 7121–7136, 1988.

Hasegawa, A., Umino, N. and Takagi, A. Double-planed structure of the deep seismic zone in the northeastern Japan arc. Tectonophysics, 47(1), pp.43-58, 1978.

Hasegawa, A., Nakajima, J., Uchida, N., Okada, T., Zhao, D., and Matsuzawa, T. Plate subduction, and generation of earthquakes and magmas in Japan as inferred from seismic observations: an overview. Gondwana Research 16 (3), 370-400. 2009.

Kaneshima, S. and Ando, M. An analysis of split shear waves observed above crustal and uppermost mantle earthquakes beneath Shikoku, Japan: Implications in effective depth extent of seismic anisotropy. Journal of Geophysical Research 94, issn: 0148-0227, 1989.

Kaneshima, S. Origin of crustal anisotropy: Shear wave splitting studies in Japan. Journal of Geophysical Research 95, issn: 0148-0227, 1990.

Lallemand, S., Heuret, A., and Boutelier, D. On the relationships between slab dip, back-arc stress, upper

plate absolute motion, and crustal nature in subduction zones. Geophysical Research Letters, 6, Q09006, 2005.

Manea, V. and Gurnis, M. Subduction zone evolution and low viscosity wedges and channels. Earth and Planetary Science Letters, 264(1), pp.22-45. 2007.

Matsuzawa, T., Umino, N., Hasegawa, A. and Takagi, A. Upper mantle velocity structure estimated from PS-converted wave beneath the north-eastern Japan Arc. Geophysical Journal International, 86(3), pp.767-787, 1986.

Matsuzawa, T., Kono, T., Hasegawa, A. and Takagi, A. Subducting plate boundary beneath the northeastern Japan arc estimated from SP converted waves. Tectonophysics, 181(1), pp.123-133, 1990.

Nakajima, J. & Hasegawa, A. Shear-wave polarization anisotropy and subduction-induced flow in the mantle wedge of northeastern Japan. Earth Planet. Sci. Lett. 225, 365-377, 2004.

Nakajima, J., Shimizu, J., Hori, S., and Hasegawa, A. Shear-wave splitting beneath the southwestern Kurile arc and northeastern Japan arc: a new insight into mantle return flow. Geophysical Research Letters, 33, L05305, 2006.

Niu, F., Levander, A., Ham, S., and Obayashi, M. Mapping the subducting Pacific slab beneath southwest Japan with Hi-net receiver functions. Earth and Planetary Science Letters, 239 (1-2), 9-17, 2005.

Tan, E., E. Choi, P. Thoutireddy, M. Gurnis, and M. Aivazis. GeoFramework: Coupling multiple models of mantle convection within a computational framework, Geochem. Geophys. Geosyst., 7, Q06001, 2006.

Tetzlaff, M. & Schmeling, H. The influence of olivine metastability on deep subduction of oceanic lithosphere. Phys. Earth. Planet. Inter. 120, 29–38, 2000.

Utsu, T. Seismicity of Japan from 1885 through 1925, Bull. Earthq. Res. Inst., Univ. Tokyo, 57 (correction and supplement), 111-117 (in Japanese with English abstract) 1982.

Usami, T. Materials for Comprehensive List of Destructive Earthquakes in Japan [416]-2001 (University of Tokyo Press), pp. 605 (in Japanese), 2003.

Yoshioka, S., and Naganoda, A. Effects of trench migration on fall of stagnant slabs into the lower mantle. Physics of the Earth and Planetary Interiors. 183(1-2), 321-329. 2010.

Zhao, D., Matsuzawa, T., and Hasegawa, A. Morphology of the subducting slab boundary in the northeastern Japan arc. Physics of the Earth and Planetary Interiors, 102(1-2), 89-104. 1997

Zhao, D., Mishra, O.P., and Sanda, R., Influence of fluids and magma on earthquakes: seismological evidence. Physics of the Earth and Planetary Interiors 132 (4), 249-267, 2002.

Zhao, D., Santosh, M., and Yamada, A. Dissecting large earthquakes in Japan: role of arc magma and fluids, Island Arc 19 (1), 4-16, 2010.

Zhong, S. and Gurnis, M. Towards a realistic simulation of plate margins in mantle convection. Geophysical Research Letters 22, issn: 0094-8276, 1995.

Zhong, S., M. T. Zuber, L. Moresi, and M. Gurnis. Role of temperature-dependent viscosity and surface plates in spherical shell models of mantle convection, J. Geophys. Res., 105(B5), 11063–11082, 2000.

**Authors:** 1) Vlad Constantin MANEA, Visiting Researcher, Research Center for Urban Safety and Security, Kobe University, Japan; 2) Shoichi YOSHIOKA, Professor, Research Center for Urban Safety and Security, Kobe University, Japan; 3) Marina MANEA, Visiting Researcher Fellow, Research Center for Urban Safety and Security, Kobe University, Japan.